Geochemistry, Geophysics, Geosystems

Supporting Information for

Subglacial geology and geomorphology of the Pensacola-Pole Basin, East Antarctica

Guy J. G. Paxman[1]*, Stewart S. R. Jamieson[1], Fausto Ferraccioli[2], Tom A. Jordan[2], Michael J. Bentley[1], Neil Ross[3], René Forsberg[4], Kenichi Matsuoka[5], Daniel Steinhage[6], Graeme Eagles[6], Tania G. Casal[7]

[1] Department of Geography, Durham University, Durham, UK
[2] British Antarctic Survey, Cambridge, UK
[3] School of Geography, Politics and Sociology, Newcastle University, Newcastle upon Tyne, UK
[4] Geodynamics, National Space Institute, Technical University of Denmark, Lyngby, Denmark
[5] Norwegian Polar Institute, Tromsø, Norway
[6] Alfred Wegener Institute Helmholtz Centre for Polar and Marine Research, Bremerhaven, Germany
[7] European Space Agency/ESTEC, Noordwijk, Netherlands

*Corresponding author: Guy J. G. Paxman (guy.j.paxman@durham.ac.uk)

Contents of this file

Introduction

This document contains details of the radio-echo sounding (RES) ice thickness and bedrock elevation data, (Figure S1 and S2), the isostatic response to ice sheet loading (Figure S3) and a comparison between forward and inverse (spectral) gravity modeling results (Figure S4 and S5 and Table S1).

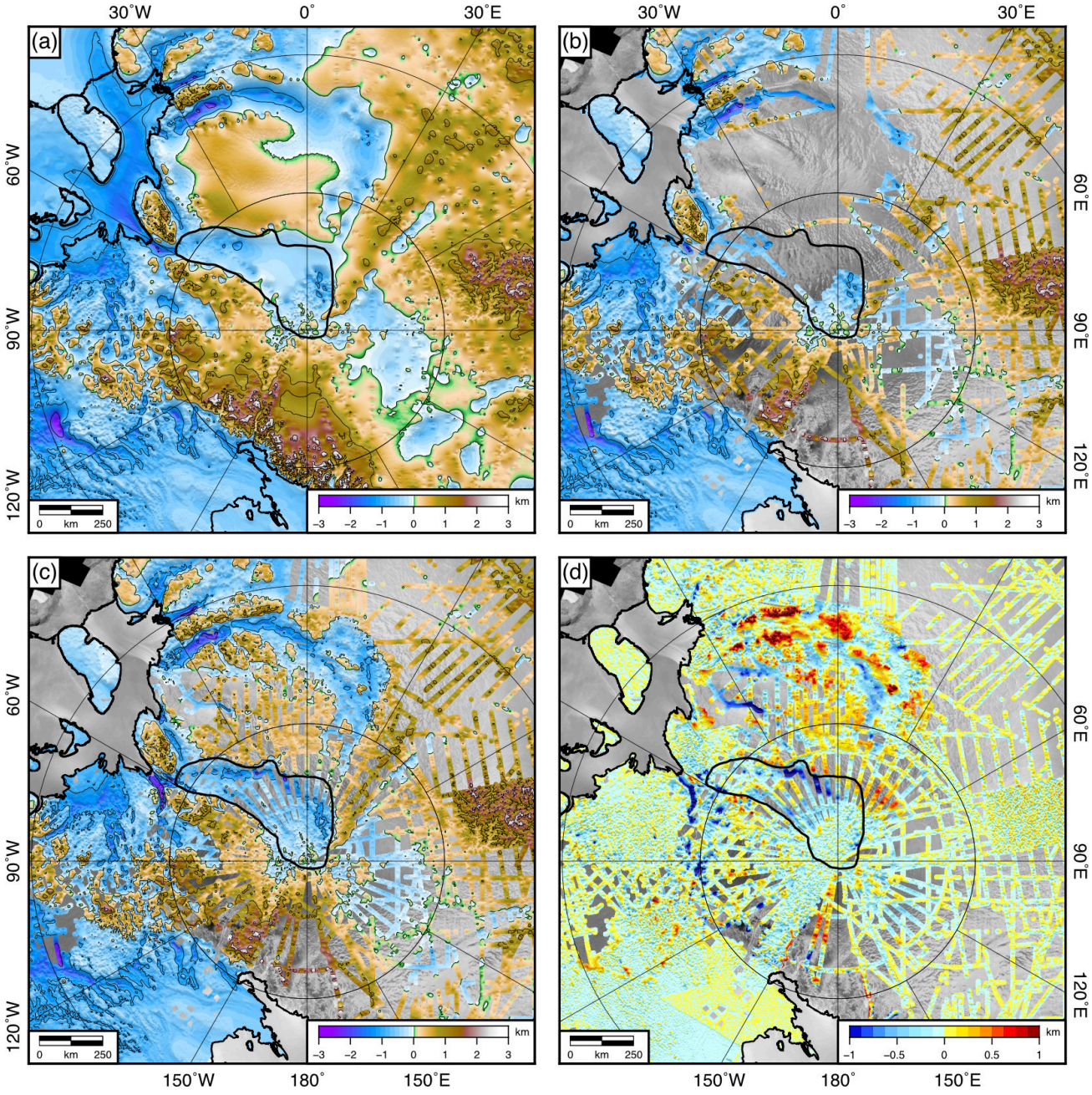

Figure S1. Comparison of the new bedrock DEM for the South Pole region with Bedmap2. (a) Bedmap2 bedrock elevation (Fretwell et al., 2013). (b) Bedmap2 bedrock elevation, masked to remove interpolated values >10 km away from the nearest RES-derived bed elevation data point. (c) New bedrock DEM, masked to remove any data >10 km away from the nearest raw RES-derived bed elevation data point. (d) Differences in bed elevation between the new DEM and Bedmap2. The largest differences occur where the PolarGAP, RECISL and ICEGRAV airborne surveys have filled former gaps in the RES data coverage. Black outline marks the Pensacola-Pole Basin.

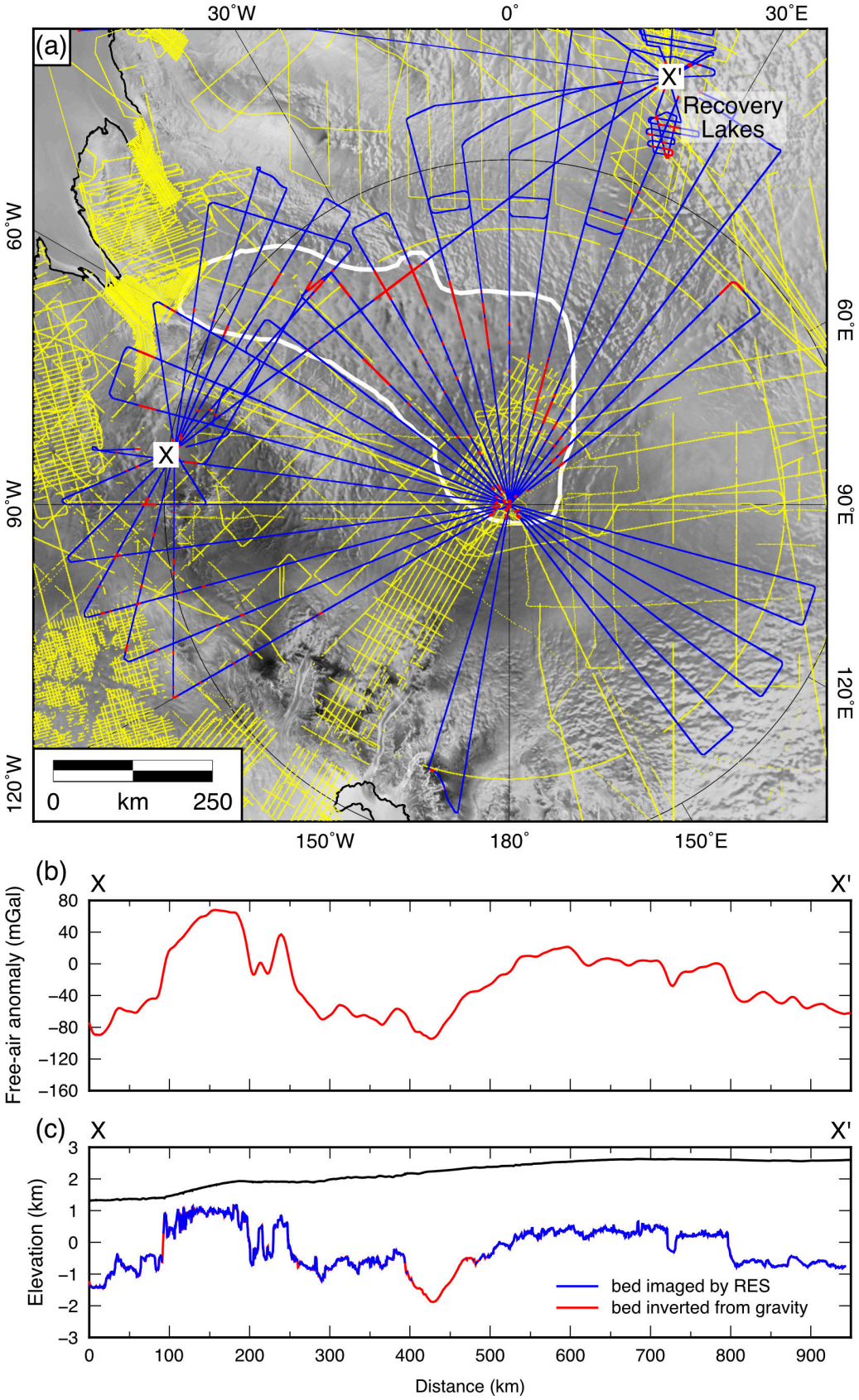

Figure S2. Inversion of bedrock elevation from gravity data. (a) Airborne geophysical data coverage over the South Pole region. Blue radial lines indicate paths flown during the 2015–16 PolarGAP survey. Red sections of these flight lines indicate areas where radio-echo sounding did not image the bed, and so the gravity inversion was used to estimate the bedrock elevation. Yellow lines show flight lines from other aerogeophysical surveys. White polygon shows the outline of the

Pensacola-Pole Basin. Small gaps (up to 10 km) in the bed in the Recovery Lakes region are likely the result of a lack of a distinct interface between ice and water in this area (Bell et al., 2007; Humbert et al., 2018; Langley et al., 2011). (b) Free-air gravity anomaly along profile X–X' (location shown in panel a). (c) Ice surface (black line) and bed (blue line) picks from radio-echo sounding are shown along with the bed inverted from the free-air gravity anomaly (red line). In our profiles and grids, we use bed picks derived from the radar data wherever they exist, and use the inverted bed from the gravity wherever there is no radar bed pick.

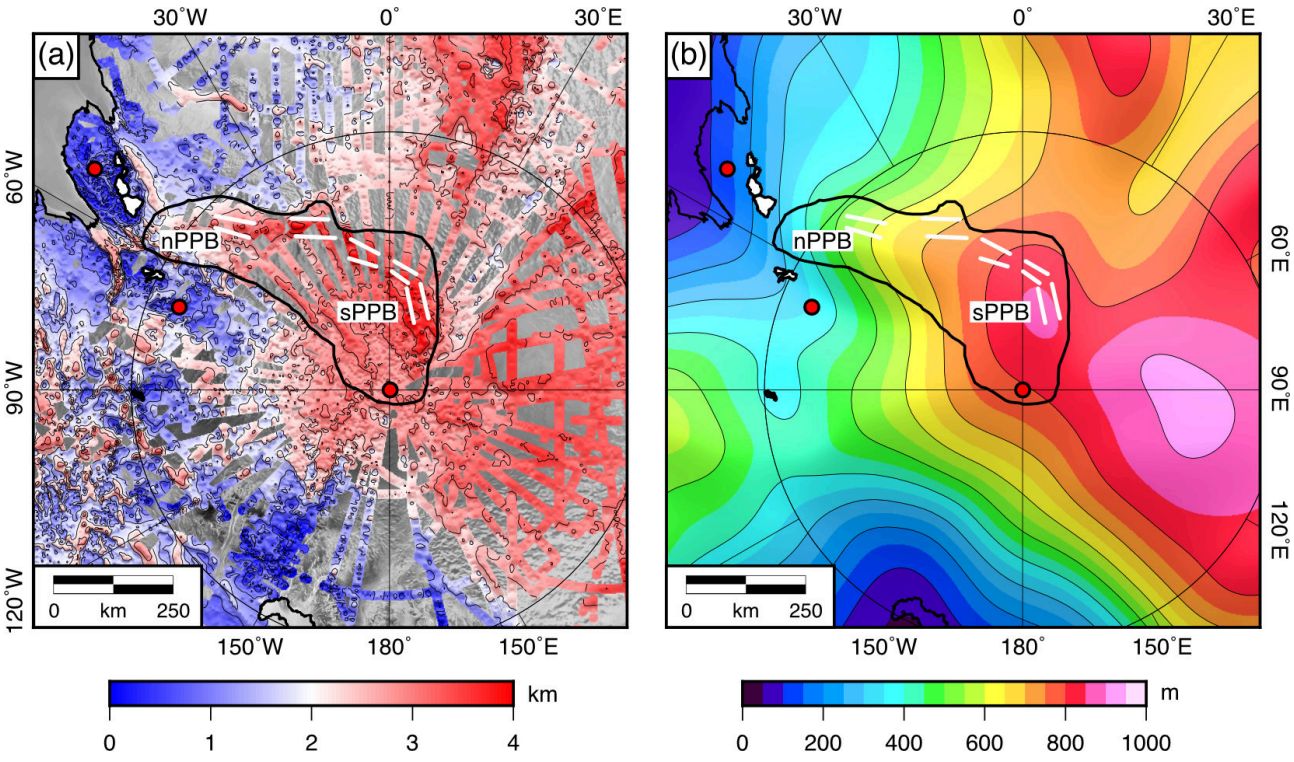

Figure S3. Isostatic rebound due to ice sheet unloading. (a) Ice thickness grid, masked to remove any data >10 km away from the nearest raw RES-derived ice thickness data point. Contour interval is 500 m. (b) Isostatic rebound due to the removal of the modern ice sheet load assuming flexural isostasy with an effective elastic thickness of 30 km. Contour interval is 100 m. Rebounding for ice sheet loading increases the difference in elevation between the higher southern PPB (sPPB) and lower-lying northern PPB (nPPB). Black outline marks the edge of the Pensacola-Pole Basin. Filled red circles show the location of seismic stations. White filled polygons outline plateau surfaces outcropping in the mountain ranges surrounding the PPB. White lines mark the outlines of overdeepened graben-like features trending along the eastern margin of the PPB.

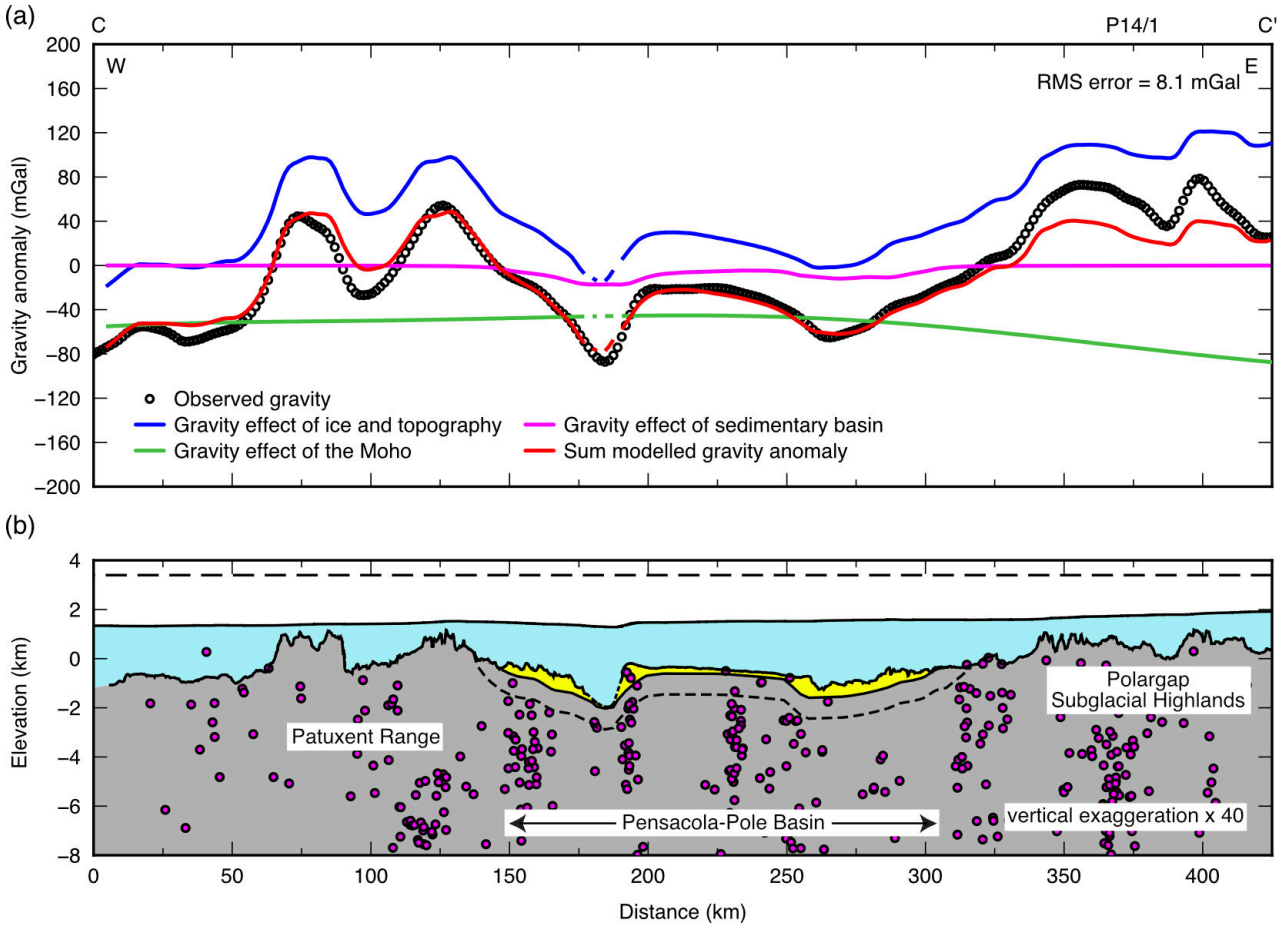

Figure S4. Gravity model along profile C–C' (location shown in Fig. 5 in the main manuscript) crossing the northern PPB. (a) Observed and calculated gravity anomalies, including modeled gravity effects of the ice and bedrock topography, the Moho, and the sedimentary basin. A long-wavelength (>1200 km) signal has been removed from the gravity field. All gravity effects were computed at 3400 m, corresponding to the maximum flight altitude / upward continuation datum for the gravity surveys (marked by the black dashed line in panel b). The root mean square (RMS) error between the observed and modeled gravity anomaly is 8.1 mGal. (b) Results of the model, showing the thickness of sedimentary rocks required to match the observed gravity 'low' over the basin. The dashed lines show the range of uncertainty of the depth of the basin based on expected variability in sediment density and effective elastic thickness. Magenta circles are estimates of the depth to magnetic source. The assumed densities of the different layers are 920 kg m^{-3} for ice (blue), 2400 kg m^{-3} for sedimentary rock (yellow), and 2670 kg m^{-3} for basement (grey). Note that the sediment thickness in this part of the basin is within the uncertainty range associated with the gravity model; gravity data are unable to resolve a significant infill of sedimentary rock in the northern PPB. We also note that there are misfits between the observed and modeled gravity anomaly near the western end of the profile, which may be indicative of similar minor (<1 km) infills of sedimentary rock, which we do not model for simplicity.

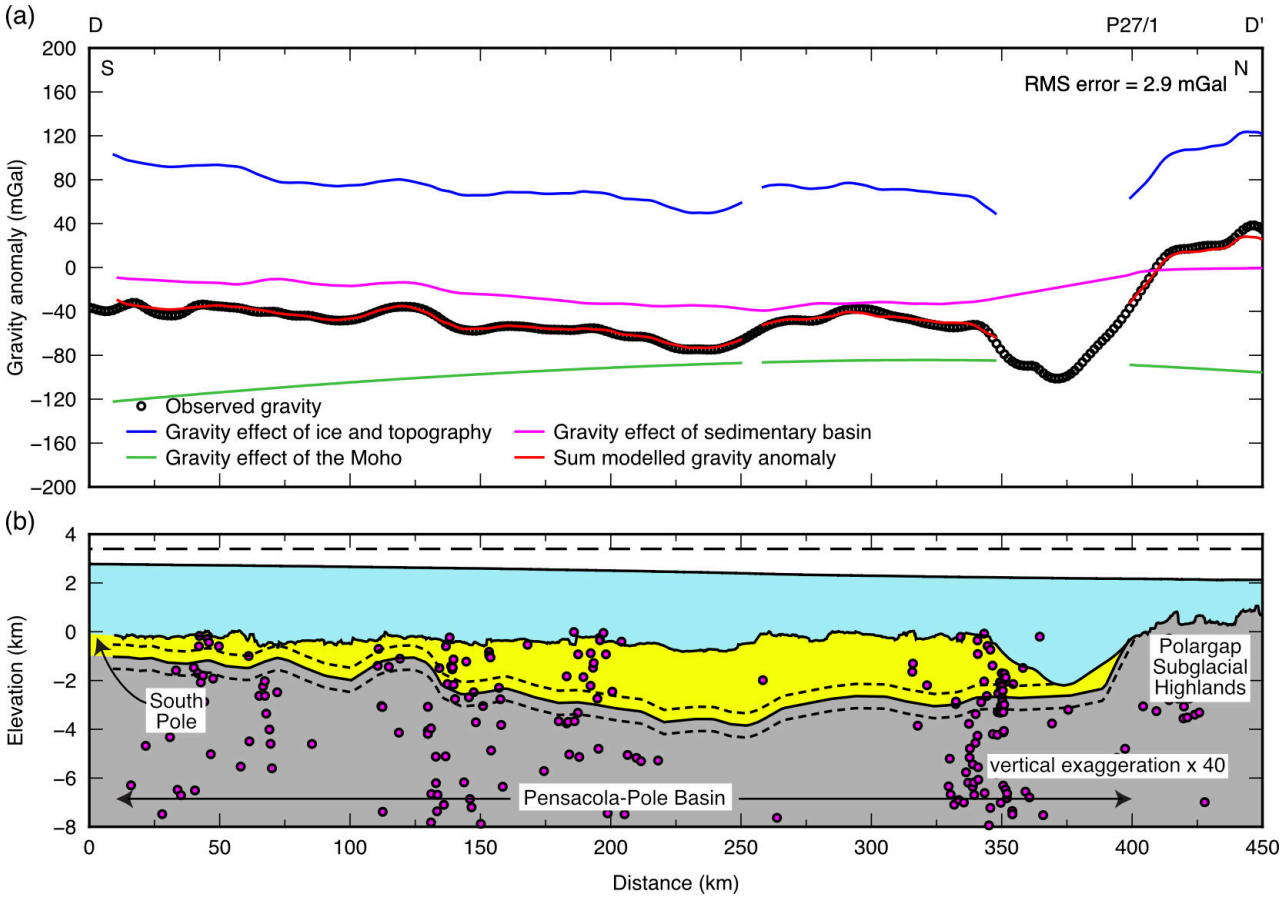

Figure S5. Gravity model along profile D–D' (location shown in Fig. 5 in the main manuscript) crossing the southern PPB. (a) Observed and calculated gravity anomalies, including modeled gravity effects of the ice and bedrock topography, the Moho, and the sedimentary basin. A long-wavelength (>1200 km) signal has been removed from the gravity field. All gravity effects were computed at 3400 m, corresponding to the maximum flight altitude / upward continuation datum for the gravity surveys (marked by the black dashed line in panel b). The root mean square (RMS) error between the observed and modeled gravity anomaly is 2.9 mGal. (b) Results of the model, showing the thickness of sedimentary rocks required to match the observed gravity 'low' over the basin. The dashed lines show the range of uncertainty of the depth of the basin based on expected variability in sediment density and effective elastic thickness. The assumed densities of the different layers are 920 kg m^{-3} for ice (blue), 2400 kg m^{-3} for sedimentary rock (yellow), and 2670 kg m^{-3} for basement (grey). Magenta circles are estimates of the depth to magnetic source. Shallow sources in the southern half of the profile may reflect intrusive Ferrar dolerites (see main manuscript). Note that there is uncertainty in the modeled sediment thickness where the bed is not imaged by the radar data, and consequently the relative gravity effects of the topography and the sedimentary basin are ambiguous.

Window Centre (Eastings, Northings in EPSG3031 Polar Stereographic projection km)	Ice thickness from power spectrum (km)	Mean ice thickness from radio-echo sounding (km)	Sediment thickness from power spectrum (km)	Mean forward model sediment thickness (km)	Maximum forward model sediment thickness (km)
(-25, 50)	2.9±0.25	3.0	1.3±0.45	1.5	3.1
(30, 70)	3.6±0.20	3.1	1.8±0.40	1.7	3.1
(0, 0)	3.3±0.25	2.9	1.4±0.45	1.3	3.1
(60, 40)	3.5±0.30	3.0	0.80±0.50	1.7	3.1
(-25, 110)	3.2±0.50	3.1	2.2±0.75	1.8	3.2
(20, 140)	3.3±0.40	3.2	2.0±0.60	1.9	3.2
(10, 180)	3.4±0.70	3.2	2.7±0.90	1.9	3.4
(-50, 180)	3.5±0.80	3.1	2.5±1.1	2.1	3.6
(-50, 220)	2.2±0.90	3.1	2.8±1.2	2.2	3.7
(-100, 220)*	3.3±0.40	3.0	3.6±1.1	2.2	3.7
(-100, 260)	3.0±0.60	2.9	3.6±1.0	2.3	3.7
(-150, 260)	3.4±0.70	2.9	4.3±1.1	2.3	3.7
(-150, 280)	2.3±0.55	2.8	3.8±0.80	2.2	3.7
(-200, 280)	2.6±0.55	2.7	3.4±0.80	2.1	3.7
(-250, 300)	2.4±0.40	2.6	3.0±0.70	1.8	3.4
(-280, 340)	2.3±0.35	2.4	3.0±0.60	1.5	3.4
(-300, 340)	2.4±0.35	2.4	2.4±0.55	1.1	3.0
(-340, 340)	2.1±0.65	2.2	1.6±0.90	0.80	3.0
(-380, 340)	2.0±0.30	2.1	1.8±0.50	0.50	2.5
(-420, 340)	2.2±0.75	2.0	0.70±0.90	0.30	1.8
	RMS difference	0.30	**RMS difference**	1.0	1.1

Table S1. Comparison of ice thickness in the PPB as determined using gravity power spectra and radio-echo sounding, and sediment thickness determined using power spectra and forward gravity models. Power spectra-derived values are given for each 200 km x 200 km window (window locations are listed from south to north, and are shown in Fig. 8a in the main manuscript). The window marked with the asterisk (*) corresponds to the spectrum shown in Fig. 8b in the main manuscript.